Memoirs of the School of Engineering, Nagoya University
Vol.45. No.1 (1993)

NUMERICAL INVESTIGATION OF PERPENDICULAR STAGED BLOWING INTO A SUBSONIC CROSS FLOW

Yoshiyuki SUGIYAMA, Masahiro YOSHIDA* and Jang-Soo CHOI

Department of Aeronautical Engineering

(Received June 1, 1993)

Abstract

Numerical solutions have been obtained for a steady viscous flow induced by a small boundary-layer blowing through three slots. The analysis is assumed to be two-dimensional, incompressible and also laminar. The analysis is made on the basis of the vorticity transport and energy equations in the conservation form, and the Poisson equation for the stream function. They are solved using the time-marching technique, together with the SOR method. The results show that a decrease in slot dia. and pitch and velocity ratio results in a reduction of the recirculating regions, but the present temperature field strongly is not affected by a recirculating flow near the blowing slots. A blowing fluid is strongly accelerated and heated by the cross flow at the leading edge of a plume. However, the stream-wise velocity component of the blowing fluid is almost constant along the plume. Moreover an increase in slot dia. or a decrease in slot pitch increases local Nusselt number and film cooling effectiveness on the slotted wall. It is also indicated that the calculated recirculating zones vary with numerical schemes used.

Nomenclature

c_f : local friction coefficient, $= \tau/(\frac{1}{2}\rho u_\infty^{*2})$
C : resultant velocity, $= \sqrt{(u^2 + v^2)}$
d : slot width, $= d^*/L^*$
h : boundary height, $= 0.8L^*/L^* = 0.8$
L : flat wall length, $= L^*/L^* = 1$
m : velocity ratio, $= v_j^*/u_\infty^*$

*Present address: Mitsubishi Motors Corporation, Okazaki

m_i : m for each slot ($i = 1,2,3$)
Nu : local Nusselt number
Pr : Prandtl number
Re : Reynolds number, $= u_\infty^* L^*/\nu$
s : slot distance (cf. Fig. 1), $= s^*/L^*$
t : time, $= t^* u_\infty^*/L^*$
T : local temperature, $= (T^* - T_j^*)/(T_\infty^* - T_j^*)$
T_j : injectant temperature, $= [T]_{T^*=T_j^*} = 0$
T_W : wall temperature, $= [T]_{T^*=T_W^*}$
T_∞ : free-stream temperature, $= [T]_{T_W^*=T_\infty^*} = 1$
u,v : stream-wise and normal velocity components, $= u^*/u_\infty^*$, $= v^*/u_\infty^*$
u_∞ : free-stream velocity, $= u_\infty^*/u_\infty^* = 1$
v_j : blowing velocity, $= v_j/u_\infty^*$
x,y : stream-wise and normal physical coordinates, $= x^*/L^*$, $= y^*/L^*$
α : weight coefficient
β : constant, $= T_W^*/T_\infty^*$
ζ : vorticity, $= \zeta^* L^*/u_\infty^*$
η_c : local cooling effectiveness, $= (T_W^* - T_\infty^*)/(T_j^* - T_\infty^*)$
ξ,η : stream-wise and normal computational coordinates
θ : $= y^* \sqrt{[u_\infty^*/(\nu x^*)]}$
ν : kinematic viscosity
ρ : density
τ : shearing stress, $= \rho\nu(\partial u^*/\partial y^*)$
ψ : stream function, $= \psi^*/(0.8 u_\infty^* L^*)$
ω : over-relaxation coefficient

Subscripts

i,j : ξ and η grid indices
KI,KJ : maximum of i and j

Superscripts

n : time index
$*$: dimensional quantity

1. Introduction

The introduction of a jet of fluid transversely into a moving stream is a basic configuration which finds application in many engineering fields. Thus, aerodynamic and heat-transfer aspects of the transverse jet have been investigated in numerous experimental, theoretical and numerical analyses. Most investigations have been made on the structure, trajectory, mixing and diffusion of the deflected transverse jet in the flow fields except around the jet hole. Parameters that were varied, included mostly velocity, momentum and temperature ratios in the previous investigations. However, there is little analytical investigation that includes a flow separation and a recirculating flow formed near the jet hole. Similarly there is little information about the effects of slot width, slot pitch and injectant split on a growth of the flow separation and the recirculating flow.

Many numerical analyses have been made on the simplified two- and three-dimensional flow fields which simulate a flow field for the film-cooling of gas-turbine blades or for the dilution air jets in gas-turbine-engine combustion chambers. However, there is still noticeable

discrepancies between calculations and experiments. We need many investigations to understand the basic aerodynamic natures of the complicated flow fields.

Bahl[1] discusses numerically the formation of the recirculating region induced by a small transverse blowing through a single porous slot in a two-dimensional flow field. However, he does not discuss any effects of the parameters on the recirculating flow. Jones, et al[5] apply a finite-difference solution procedure to a round turbulent jet into a confined cross-flow. The calculated results are in qualitative agreement with experiments because the standard $k-\epsilon$ model used is probably inadequate. They do not discuss basic aerodynamic natures of the induced vortex flow and the deflected jet and the effects of the geometric configuration on the jet and vortex flows. Bergeles, et al[6] use a three-dimensional finite-difference procedure to predict the flow and thermal fields arising from discrete jets issuing transversely into an external stream. A laminar and partially parabolic flow is assumed. Therefore, we can not know the vortex flow field around the jet holes. Bergeles, et al[7] report a cooling effectiveness which is obtained by a simulation of the injection into a hot gas cross-flow through a row of downstream-facing holes. A turbulent flow is assumed and is with the effect of turbulence modelled in a way which allows for the anisotropies. Comparisons with measurements show good agreement in the majority of the calculated cases for the cooling effectiveness. However, discrepancies are observed at small upstream boundary layer thickness or large injection rates. The basic aerodynamic natures are not shown.

This paper analyzes numerically a flow induced by a small blowing through three solts built in a stream-wise plane wall. The present flow field is a model for that associated with a film cooling of gas-turbine blades and combustor liners. The analysis is assumed to be two-dimensional, incompressible, and also laminar to exclude an ambiguity introduced by an uncertain turbulence model into the analysis, because the turbulence of the present flow field is not simple enough to be expressed by only a single model. Laminar flow predictions have at least some practical relevance for flow over turbine blades because the very strong accelerations which occur over the blade prevent or delay the boundary layer becoming turbulent. The governing equations are solved numerically with a well known time-marching technique. The object of the present paper is to show effects of various parameters on the flow field including a boundary-layer separation and a recirculating flow which influence the heat transfer. Parameters that are varied, include slot pitch, slot width, velocity ratio and injectant split. Considerations are still needed for a numerical treatment of a singular point at slot edges in order to increase a velocity ratio (=blowing velocity at exit/cross-flow velocity). However, the present analysis gives qualitatively reasonable results.

2. Analysis

Governing Equations. The flow and temperature fields for a transverse boundary-layer blowing (Fig. 1) are governed by the vorticity transport equation, the Poisson equation for the stream function and the energy equation. Written in conservation law form for two-dimensional coordinates, these equations are expressed as, in the absence of body force and in the non-dimensional form,

$$\frac{\partial \zeta}{\partial t}+\frac{\partial (u\zeta)}{\partial x}+\frac{\partial (v\zeta)}{\partial y}=\frac{1}{Re}\left(\frac{\partial^2 \zeta}{\partial x^2}+\frac{\partial^2 \zeta}{\partial y^2}\right), \tag{1}$$

$$\frac{\partial^2 \psi}{\partial x^2}+\frac{\partial^2 \psi}{\partial y^2}=-\zeta, \tag{2}$$

$$\frac{\partial T}{\partial t}+\frac{\partial(uT)}{\partial x}+\frac{\partial(vT)}{\partial y}=\frac{1}{RePr}\left(\frac{\partial^2 T}{\partial x^2}+\frac{\partial^2 T}{\partial y^2}\right), \tag{3}$$

where $u=\partial\psi/\partial y$ and $v=-\partial\psi/\partial x$. For simplicity of the present analysis the specific heat and the laminar viscosity are assumed to be constant.

Boundary conditions. Boundary conditions are set by referring to Fig. 1.

i) At the slotted wall "OC",

$$u\equiv\partial\psi/\partial y=0\,,\quad v\equiv-\partial\psi/\partial x=\delta_1 m_i\,,\quad T=\delta_2\beta \text{ or } \partial T/\partial y=0\,,$$

where $\delta_1=0$ and $\delta_2=1$ on the wall, and $\delta_1=1$ and $\delta_2=0$ at the three slots. The present analysis is made on both isothermal and adiabatic walls. At the slots the boundary conditions are specified by fixing all the dependent variables at their initial values which are uniform across the slots.

ii) At the inflow boundary "OA",

$$\psi=y(u\equiv\partial\psi/\partial y=1\,,\quad v\equiv-\partial\psi/\partial x=0)\,,\quad \zeta=0\,,\quad T=1\,.$$

It is assumed that the blowing does not influence the inflow boundary conditions.

iii) At the upper boundary "AB" we assume a slip wall without a boundary layer so that,

$$\partial\psi/\partial y=1\,,\quad \partial\psi/\partial x=0\,,\quad \partial\zeta/\partial y=0\,,\quad \partial T/\partial y=0\,,\quad T=1\,.$$

iv) At the outflow boundary "BC" all dependent variables are calculated by a linear extrapolation from the upstream values.

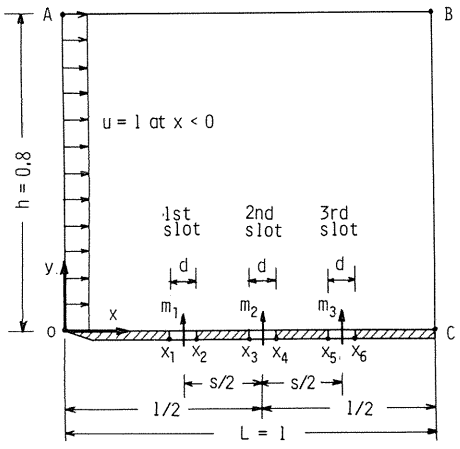

Fig. 1 Model problem for flow field affected by staged transverse blowing through porous slots.

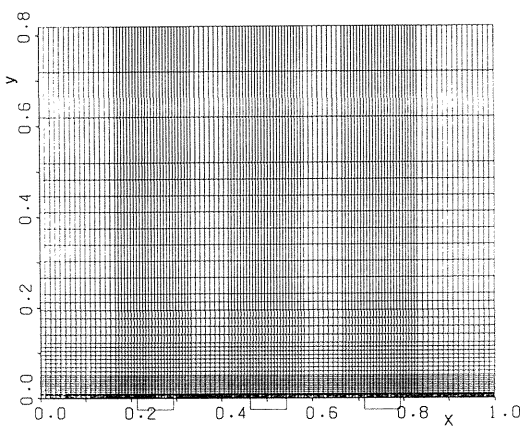

Fig. 2 Grid (122 × 43).

Coordinate transformation. Equations (1) through (3) are transformed from the physical domain (x,y,t) with a non-uniform grid to the computational one (ξ,η,t) with a uniform grid using the independent variable transformation, $x=f(\xi)$ and $y=g(\eta)$, which are numerically given. Functions, $x=f(\xi)$ and $y=g(\eta)$ are defined to obtain the compression of the grid near the slots and the slotted wall (Fig. 2). The quantities $\partial\zeta/\partial x$, $\partial\zeta/\partial y$, $\partial^2\zeta/\partial x^2$ and $\partial^2\zeta/\partial y^2$ appear in the governing equations. These are given by the following: The partial derivative $\partial\zeta/\partial\xi$ is equal to $(\partial\zeta/\partial x)(dx/d\xi)$ so that we have $\partial\zeta/\partial x = (df/d\xi)^{-1}(\partial\zeta/\partial\xi)$. In the same way $\partial\zeta/\partial y = (dg/d\eta)^{-1}(\partial\zeta/\partial\eta)$. The second partial derivative $\partial^2\zeta/\partial\xi^2$ is equal to $(\partial^2\zeta/\partial x^2)(df/d\xi)^2 + (\partial\zeta/\partial x)(d^2f/d\xi^2)$. This becomes the expression $\partial^2\zeta/\partial x^2 = (df/d\xi)^{-2}\{\partial^2\zeta/\partial\xi^2 - (df/d\xi)^{-1}(d^2f/d\xi^2)(\partial\zeta/\partial\xi)\}$, and similarly $\partial^2\zeta/\partial y^2 = (dg/d\eta)^{-2}\{\partial^2\zeta/\partial\eta^2 - (dg/d\eta)^{-1}(d^2g/d\eta^2)(\partial\zeta/\partial\eta)\}$. After substituting these quantities into eqs. (1) to (3), these equations are expressed as,

$$\frac{\partial\zeta}{\partial t}+\frac{\partial(u\zeta)}{\partial\xi}\left(\frac{df}{d\xi}\right)^{-1}+\frac{\partial(v\zeta)}{\partial\eta}\left(\frac{dg}{d\eta}\right)^{-1}$$
$$=\frac{1}{Re}\left(\frac{df}{d\xi}\right)^{-2}\left\{\frac{\partial^2\zeta}{\partial\xi^2}-\left(\frac{df}{d\xi}\right)^{-1}\frac{d^2f}{d\xi^2}\frac{\partial\zeta}{\partial\xi}\right\}$$
$$+\left(\frac{dg}{d\eta}\right)^{-2}\left\{\frac{\partial^2\zeta}{\partial\eta^2}-\left(\frac{dg}{d\eta}\right)^{-1}\frac{d^2g}{d\eta^2}\frac{\partial\zeta}{\partial\eta}\right\}, \tag{4}$$

$$\left(\frac{df}{d\xi}\right)^{-2}\left\{\frac{\partial^2\psi}{\partial\xi^2}-\left(\frac{df}{d\xi}\right)^{-1}\frac{d^2f}{d\xi^2}\frac{\partial\psi}{\partial\xi}\right\}$$
$$+\left(\frac{dg}{d\eta}\right)^{-2}\left\{\frac{\partial^2\psi}{\partial\eta^2}-\left(\frac{dg}{d\eta}\right)^{-1}\frac{d^2g}{d\eta^2}\frac{\partial\psi}{\partial\eta}\right\}=-\zeta, \tag{5}$$

where

$$u=\left(\frac{dg}{d\eta}\right)^{-1}\frac{\partial\psi}{\partial\eta},\quad v=-\left(\frac{df}{d\xi}\right)^{-1}\frac{\partial\psi}{\partial\xi}, \tag{6}$$

and

$$\frac{\partial T}{\partial t}+\frac{\partial(uT)}{\partial\xi}\left(\frac{df}{d\xi}\right)^{-1}+\frac{\partial(vT)}{\partial\eta}\left(\frac{dg}{d\eta}\right)^{-1}$$
$$=\frac{1}{RePr}\left(\frac{df}{d\xi}\right)^{-2}\left\{\frac{\partial^2T}{\partial\xi^2}-\left(\frac{df}{d\xi}\right)^{-1}\frac{d^2f}{d\xi^2}\frac{\partial T}{\partial\xi}\right\}$$
$$+\left(\frac{dg}{d\eta}\right)^{-2}\left\{\frac{\partial^2T}{\partial\eta^2}-\left(\frac{dg}{d\eta}\right)^{-1}\frac{d^2g}{d\eta^2}\frac{\partial T}{\partial\eta}\right\}. \tag{7}$$

Method of solution. The explicit, time-marching technique is used to integrate the governing equations until a steady-state solution is reached. A difference form of the convective terms of eqs. (4) and (7) is expressed by the combination of [2nd order central difference + α (1st order upwind difference $-$2nd order central difference)] for each convective term.

Assuming $\psi^n_{i,j}$, we can obtain $\zeta^n_{i,j}$ from the difference form of eq. (5). Substituting $\zeta^n_{i,j}$ into

the difference form of eq. (4), we get $\zeta_{i,j}^{n+1}$. Replacing n by $n+1$ in the difference form of eq. (5), and expressing explicitly $\psi_{i,j}^{n+1}$, we have the following simultaneous equations for the unknown $\psi_{i,j}^{n+1}$'s to be solved through the SOR method.

$$\psi_{i,j}^{n+1} = \left\{\frac{8}{(f_{i+1}-f_{i-1})^2} + \frac{8}{(g_{j+1}-g_{j-1})^2}\right\}^{-1} \cdot \left[8\left\{\frac{(f_i - f_{i-1})\psi_{i+1,j}^{n+1} + (f_{i+1}-f_i)\psi_{i-1,j}^{n+1}}{(f_{i+1}-f_{i-1})^3}\right\} + 8\left\{\frac{(g_j - g_{j-1})\psi_{i,j+1}^{n+1} + (g_{j+1}-g_j)\psi_{i,j-1}^{n+1}}{(g_{j+1}-g_{j-1})^3}\right\} + \zeta_{i,j}^{n+1}\right]. \tag{8}$$

In the calculation of $\psi_{i,j}^{n+1}$ we start at the slotted boundary "OC" (cf. Fig. 1) and sweep up by rows (j's). Thus we can replace $\psi_{i+1,j}^{n+1}$, and $\psi_{i,j+1}^{n+1}$ in eq. (8) by $\psi_{i+1,j}^{n}$ and $\psi_{i,j+1}^{n}$ to obtain an approximation of $\psi_{i,j}^{n+1}$ designated by $\tilde{\psi}_{i,j}^{n+1}$. When $\psi_{i,j}^{k}$ and $\psi_{i,j}^{k+1}$ show the approximations of $\psi_{i,j}^{n+1}$ obtained at the k and $k+1$ iteration levels respectively, a SOR step becomes

$$\tilde{\psi}_{i,j}^{k+1} = \left\{\frac{8}{(f_{i+1}-f_{i-1})^2} + \frac{8}{(g_{j+1}-g_{j-1})^2}\right\}^{-1} \cdot \left[8\left\{\frac{(f_i - f_{i-1})\psi_{i+1,j}^{k} + (f_{i+1}-f_i)\psi_{i-1,j}^{k+1}}{(f_{i+1}-f_{i-1})^3}\right\} + 8\left\{\frac{(g_j - g_{j-1})\psi_{i,j+1}^{k} + (g_{j+1}-g_j)\psi_{i,j-1}^{k+1}}{(g_{j+1}-g_{j-1})^3}\right\} + \zeta_{i,j}^{k+1}\right],$$

$$\psi_{i,j}^{k+1} = \psi_{i,j}^{k} + \omega(\tilde{\psi}_{i,j}^{k+1} - \psi_{i,j}^{k}).$$

The converging values of $\psi_{i,j}^{k+1}$ give $\psi_{i,j}^{n+1}$ from which we can obtain corrective values of $\zeta_{i,j}^{n+1}$. When $\zeta_{i,j}^{n+1}$ can not satisfy the converging condition, Δt in the difference form of eq. (4) is calculated to advance the time level n.

The energy equation (3) has the same form as the vorticity transport equation (1). The difference representation of eq. (3) is obtained by replacing ζ and Re in the difference representation of eq. (1) by T and the product $Re\,Pr$, respectively.

To insure numerical stability, the time step Δt associated with the difference form of eq. (1) is shown to be limited to at least

$$\Delta t \le \left\{2\nu\left(\frac{1}{\Delta x^2} + \frac{1}{\Delta y^2}\right) + \frac{|u|}{\Delta x} + \frac{|v|}{\Delta y}\right\}^{-1}, \tag{9}$$

as shown in ref.3). However, we take the other way for the estimation of Δt[2]. Using the stability restriction deduced from FTCS differencing of eq. (1), we get

$$\Delta t \le \frac{\Delta x^2 \Delta y^2}{2(\Delta x^2 + \Delta y^2)} Re, \tag{10}$$

where for eq. (3) Re is replaced by the product $Re\,Pr$, and

$$\Delta t \leq \left(\frac{u}{\Delta x}+\frac{v}{\Delta y}\right)^{-1}. \tag{11}$$

For simplicity we use the following instead of eq. (11),

$$\Delta t \leq \frac{1}{2}\frac{\Delta x}{u_{max}} \quad \text{and} \quad \Delta t \leq \frac{1}{2}\frac{\Delta y}{v_{max}}, \tag{11'}$$

where u_{max} and v_{max} are the maximum u and v in the present flow field. We use as the maximum time step Δt_{max} the factor of 0.8 times the minimum value of three Δt's given by eqs. (10) and (11'). Δt_{max} optimally renewed in the present code is about 3.45×10^{-3}. The Δt_{max} for eq. (3) is kept constant 3.5×10^{-3}.

The flow field is spanned by a finite difference grid with 122 nodes in the stream-wise direction and 43 nodes in the normal direction (cf. Fig. 2). The grid is geometrically stretched away from the wall, and unchanged crossflow-wise, but fine in the slot region. The relaxation coefficient ω is given by $\omega = 2\{1 - \sqrt{1 - (A/4)}\}/(A/4)$, where $A = \{\cos(\pi/KI) + \cos(\pi/KJ)\}^2$. We use ω=1.896 for KI=122 and KJ=43 and α=0.65.

The local coefficient of skin friction c_f is calculated by

$$c_f = (\tau)_{wall}/(\tfrac{1}{2}\rho u_\infty^{*2}) = (2/Re)(\partial u/\partial y)_{wall} \tag{12}$$

on the slotted wall.

The local Nusselt number Nu is given by

$$Nu = \alpha_x^* L^*/\lambda = -(\partial T/\partial y)_{wall}/(1 - T_w), \tag{13}$$

where α_x^* shows local heat-transfer coefficient and λ thermal conductivity of the wall substance.

A local film cooling effectiveness η_c is defined by

$$\eta_c = (T_W^* - T_\infty^*)/(T_j^* - T_\infty^*) = 1 - T_W. \tag{14}$$

3. Results

The validity of the program is demonstrated in a no-blowing condition. When the Blasius velocity profile is given at the inflow boundary, at the outflow boundary the deviation is within 3% from the Blasius profile. However, when the uniform velocity profile is used instead of the Blasius profile, the deviation is within 7%. An average Nusselt number over the wall agrees fairly well with the known value for the laminar flow without the blowing[4]. The calculations of ζ converge perfectly after a non-dimensional time t=6 to 8.

The configuration of the present flow field calculated is shown in Fig. 1, where L^*=0.4 m, h=0.8, u_∞^*=1 m/s. An injectant issues from the slots of d=0.08 or 0.053, and

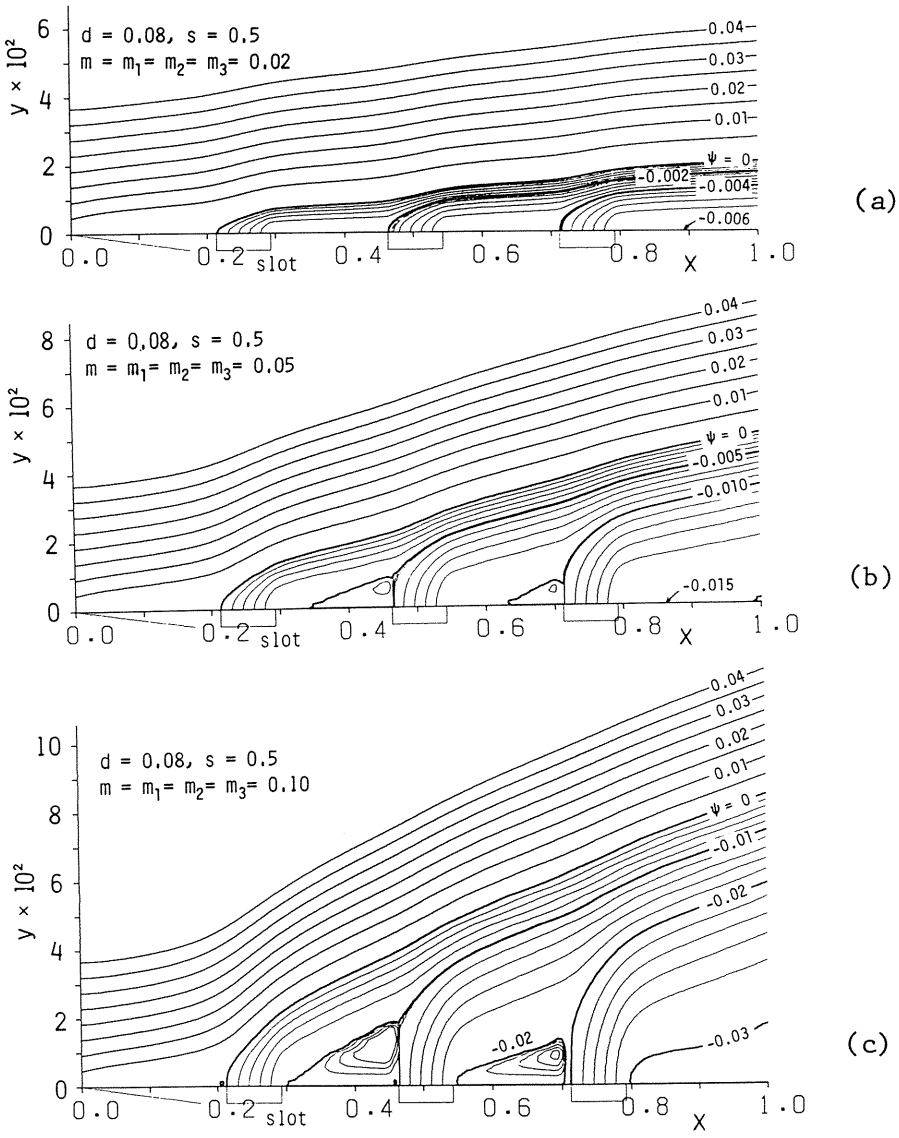

Fig. 3 Streamlines for transverse blowing at various velocity-ratios, showing vortex formation.

s=0.5 or 0.41. Flow characteristics are calculated, at m=0.02, 0.05 and 0.1, and T_∞=1, T_j=0 and β=0.5 in each combination of d and s at Pr=1 and Re=26666 for air.

Fig. 3 shows an example of the effects of m on the recirculating regions between the slots. The expected features of the flow field have been predicted by the simulations. The recirculating region between slots is smaller in the downstream part of the wall than in the upstream part at a given m, but expands as m increases. The recirculating region appears upstream of the 1st slot, when the velocity ratio or the slot width of the 1st slot is large. Bahl[1)]

shows production of a recirculating region with two cells which counterrotate just upstream of a single slot. However, the present analysis does not reveal such a sign. Parametric calculations have revealed that the recirculating regions between the slots reduce in the case of d=0.08 and s=0.41 or d=0.053 and s=0.5 in comparison with the case of d=0.08 and s=0.5. This shows that a decrease in s or d results in a reduction of the recirculating regions.

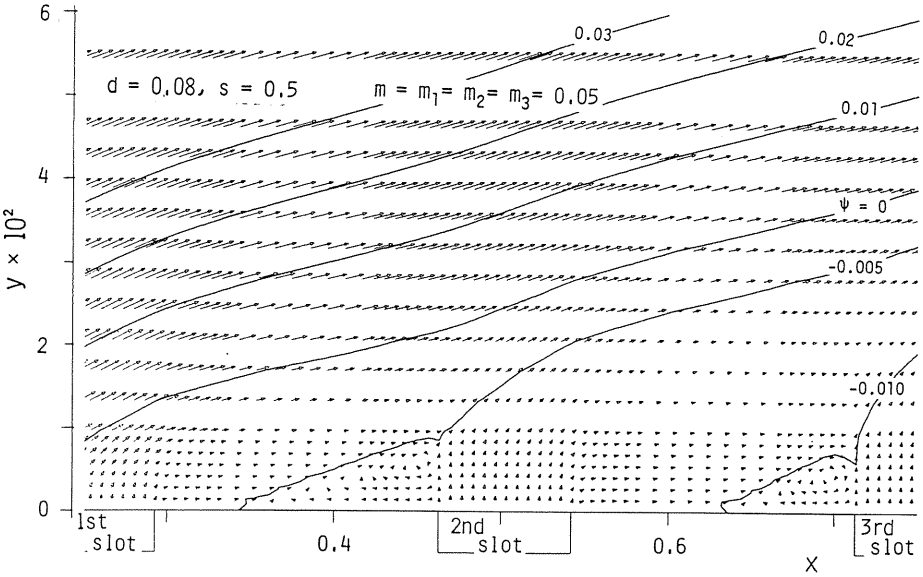

Fig. 4 Magnified velocity-vector diagram showing vortex flow.

Fig. 4 shows an example of a magnified vector plot with the streamlines near the slotted wall. We find the recirculating flows just upstream of the 2nd and 3rd slots. The recirculation is indicated by a reversal of the velocity vectors. However, there are no two cells in the recirculating region shown by Bahl[1].

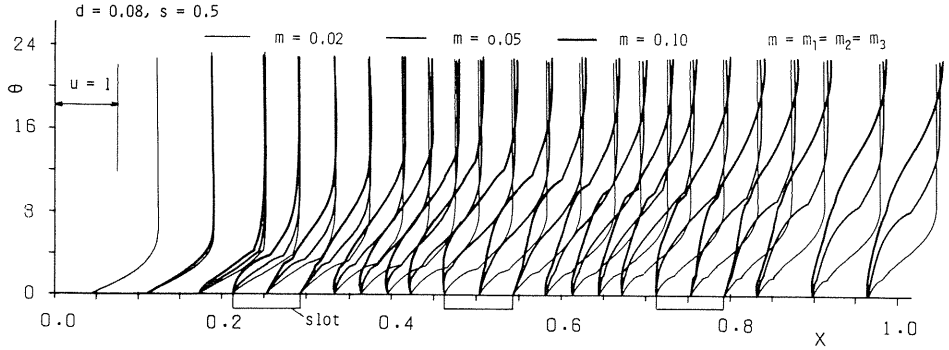

Fig. 5 Velocity distributions of boundary layer on slotted wall.

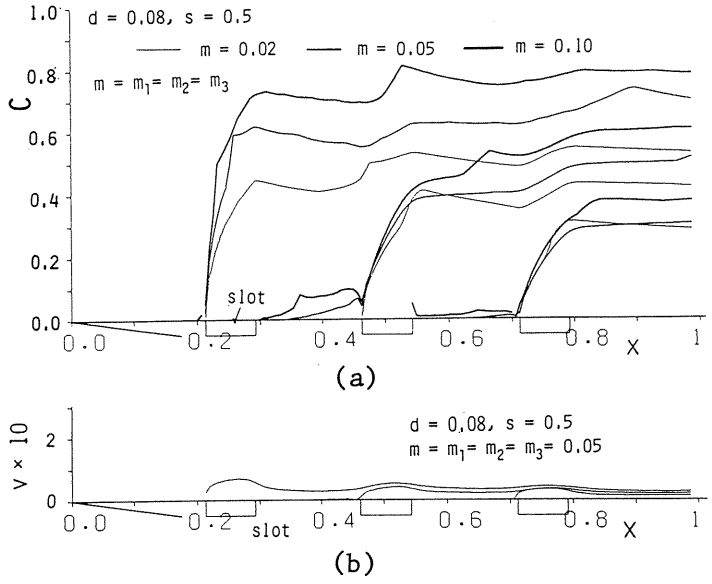

Fig. 6 Variations of velocity along each streamline through leading edge of slot exits.

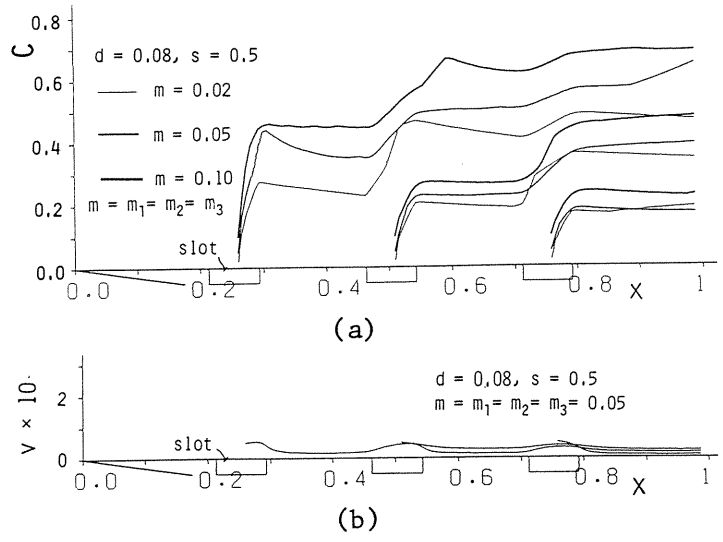

Fig. 7 Variations of velocity along each streamline through center of slot exits.

Fig. 5 shows effects of m on the boundary-layer velocity profile. As expected, $(\partial u/\partial y)_{wall}$ diminishes with increasing m on and around the slots. However, $(\partial u/\partial y)_{wall}$ is smaller on the 2nd and 3rd slots than on the 1st slot. At m=0.02, $(\partial u/\partial y)_{wall}$ is nearly unchanged on and around the three slots. At m=0.05 and 0.1, $(\partial u/\partial y)_{wall}$ becomes almost zero just near the leading edge of the 2nd and 3rd slots, but this does not appear at m=0.02. A tendency to a flow separation is suppressed on the slots and this is clear on the 2nd and 3rd slots at m=0.05 and 0.1. The reverse-flow regions near the wall are clearly found in the velocity distributions between the 1st and 2nd slots at m=0.05 and 0.1 and in that between the 2nd and 3rd slots at m=0.1. $(\partial u/\partial y)_{wall}$ is large upstream of the 1st slot, but becomes nearly zero everywhere downstream of the 1st slot.

Figs. 6 (a) and (b) and Figs. 7 (a) and (b) show variations of C and v along the streamlines issuing from the leading edge and center of the slots, respectively. A plot of u is not shown here, because the plots of C and u against x are nearly equal except a small difference near the slot. The small difference results from that the plot of C against x starts from the slot-exit velocity, but the plot of u against x starts from zero velocity. The velocity C is larger along the plume leading-edge than in its inside (cf. Figs. 6 (a) and 7 (a)). This shows that the plume fluid is accelerated along the plume by the cross flow. There is a small effect of m on the velocity along the plume discharged from the 3rd slot. The plot of C against x for the 1st

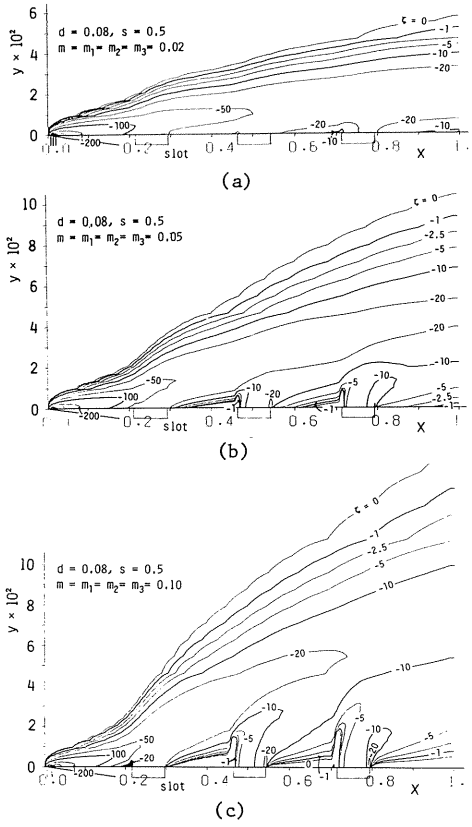

Fig. 8 Variations of vorticity distribution with increasing velocity ratio.

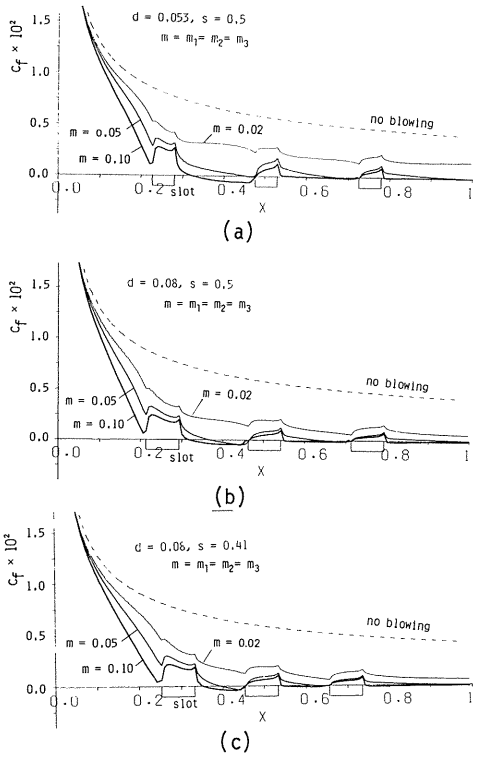

Fig. 9 Variations of local friction coefficient along slotted wall.

slot shows that after C reaches its first peak, C keeps the peak value until the effect of the 2nd slot becomes predominant. This behavior is almost the same, even though m varies. The normal velocity component v in Figs. 6 (b) and 7 (b) does not vary between slots and is large only at the slot exit.

Fig. 8 shows effects of m on ζ. A peak of $|\zeta|$ occurs almost along the streamline of $\psi=0$ except in the nearfield of the wall leading-edge (cf. Fig. 3), and starts from a large $|\zeta|$ region near the wall leading-edge. We can assume the peak of $|\zeta|$ to be a boundary which separates the influence region of the wall boundary layer upstream of the 1st slot from that of the injectant. The large vorticity indicates a place where a strong viscous diffusion occurs. The vorticity $|\zeta|$ is not necessarily large around the slot leading and trailing edges against the large $|\zeta|$ upstream of the lst slot. We can also see that a central part of the recirculating region is not necessarily in a large $|\zeta|$, and that there is a relatively large $|\zeta|$ in a place where a large velocity gradient is expected.

Fig. 9 shows variations of friction coefficient (eq. (12)) along the wall with m, d and s, including c_f of the no-blowing wall calculated by the present code. There is a continuous decrease in c_f upstream of the 1st slot due to blowing and the decrease becomes great with increasing m. c_f is smaller on the 2nd and 3rd slots than on the 1st one. There is a rapid increase in c_f at the leading edge of the 1st slot as m increases, but this is not found for the 2nd and 3rd slots. c_f is almost the same downstream of the 2nd and 3rd slots at m=0.05 and 0.1, but is very large at m=0.02. This means that the wall boundary layer reaches separation downstream of the 2nd and 3rd slots at about $m \simeq 0.1$. We find the negative c_f, which means a reverse flow, in the region between the 1st and 2nd slots. c_f plottings show it to be

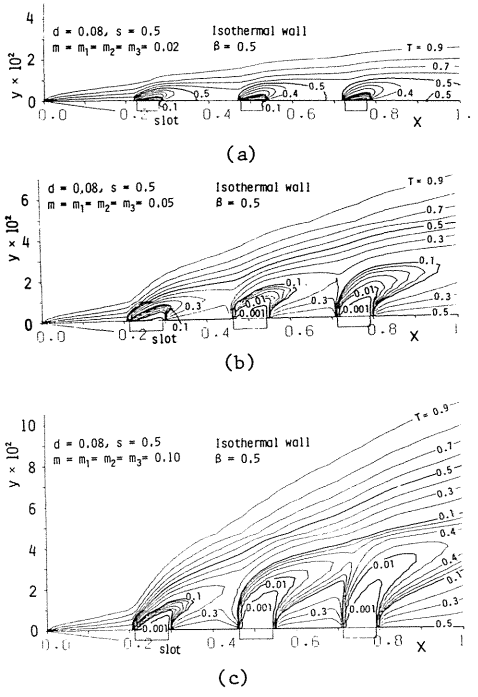

Fig. 10 Temperature distributions affected by isothermal wall with slots at various velocity ratios.

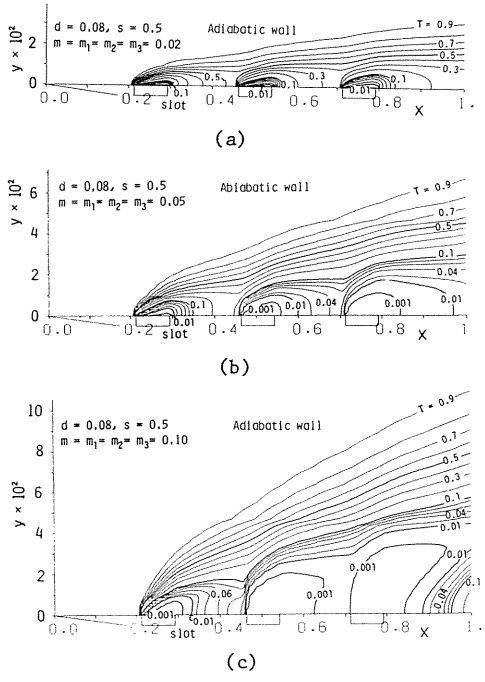

Fig. 11 Temperature distributions affected by adiabatic wall with slots at various velocity ratios.

qualitatively independent of the present combinations of d and s. A comparison of Figs. 9 (a) and (b) indicates the effects of d on c_f. Noticeable points are: (1) When m is increased, the decrease in c_f is slower at d=0.053 than at d=0.08. This is obvious downstream of the 1st slot. (2) The configuration with a small d retards separation of the wall boundary layer, or results in a small recirculation zone.

A comparison of Figs. 9 (b) and (c) indicates the effects of s on c_f. We can assume that the variation of s has little influence on c_f. It is consequently concluded that the magnitude of d has a predominant effect on c_f through the flow rate of the injectant.

Figs. 10 and 11 show isotherms of the flow field affected by the isothermal and adiabatic walls, respectively. Fig. 3 shows the flow fields which give the temperature fields in Figs. 10 and 11. In Fig. 10 a thermal diffusion is greater in the plume issuing from the upstream slot than from the downstream one. Penetration of isotherms increases across each slot exit from its leading edge to its trailing one. This means that the cross flow heats the injectant. The analysis shows a little effect of the recirculating flow on the isotherms near the slotted wall. We can point out this little effect as follows: There is the recirculating flow in Figs. 3 (b) and (c), but not in Fig. 3 (a). The difference between the flow fields results in a formation of the roofshaped isotherms near the wall between the slots (cf. Fig. 10 (b) or (c)).

Fig. 11 does not indicate clearly the effects of the recirculating flow on the isotherms. However, it is noticeable that at m=0.1 a thermal diffusion is very slow in the plume issuing from the 2nd and 3rd slots compared with that from the 1st slot, as indicated by the isotherm of T=0.001. The low thermal diffusion is attributed to an accumulation of the low-temperature injectant near the adiabatic wall.

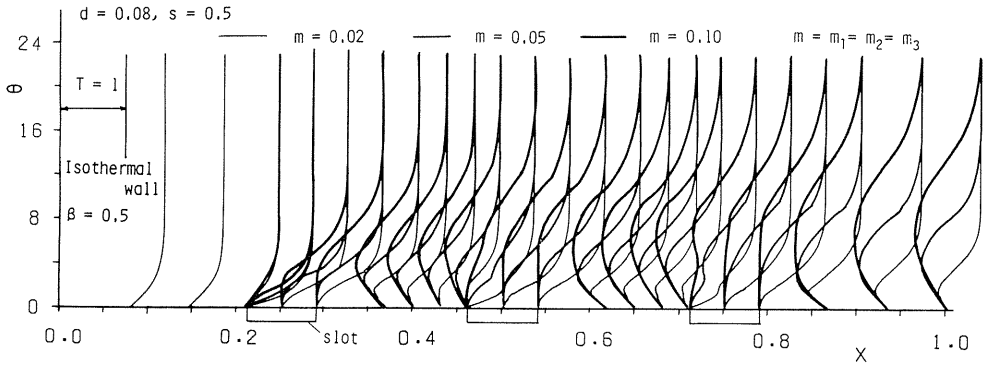

Fig. 12 Temperature distributions of thermal boundary layer on slotted wall.

Fig. 12 shows the expected effects of the injectant from the three slots on the temperature profile of the boundary layer on the isothermal wall at various m's. The temperature profiles between the slots and in the downstream region of the 3rd slot have a low temperature part, which expands with increasing m. This part corresponds to a flow passage of the injectant and the location of the minimum temperature goes away from the wall as m increases (cf. Fig. 10). On the other hand we find that a uniform temperature core is formed in the flow passage of the injectant near its exit. Such a uniform temperature core is larger in the downstream slot than in the upstream one and is greater at large m than at small m.

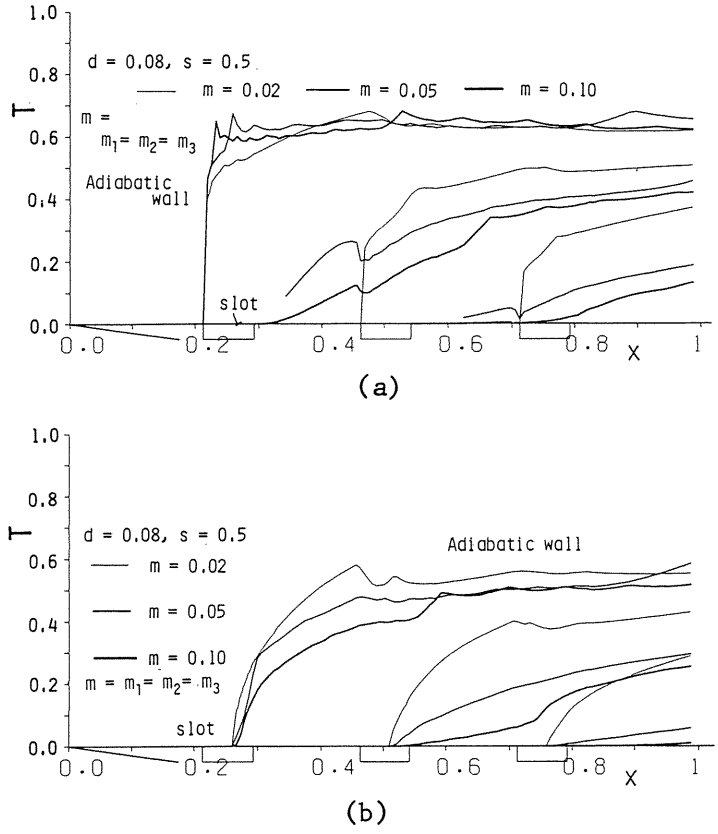

Fig. 13 Variations of temperature along streamline through
(a) leading edge of slot exits, and
(b) center of slot exits.

Figs. 13 (a) and (b) show variations of temperature along the streamlines issuing from the leading edge and center of the slots, respectively. Fig. 13 (a) shows that the injectant is rapidly heated by the cross flow after issuing from the leading edge of the 1st slot, and then keeps a nearly constant temperature. However, there is an asymptotic change of temperature along the streamlines issuing from the 2nd and 3rd slots. Fig. 13 (b) shows that the injectant from the 1st slot is slowly heated by the cross flow in comparison with the case of Fig. 13 (a). This is attributed to the fact that the cross flow cannot quickly heat the inner part of the plume.

Temperature along both the streamlines diminishes with the increase in m, except along the streamlines from the 1st slot in Fig. 13 (a).

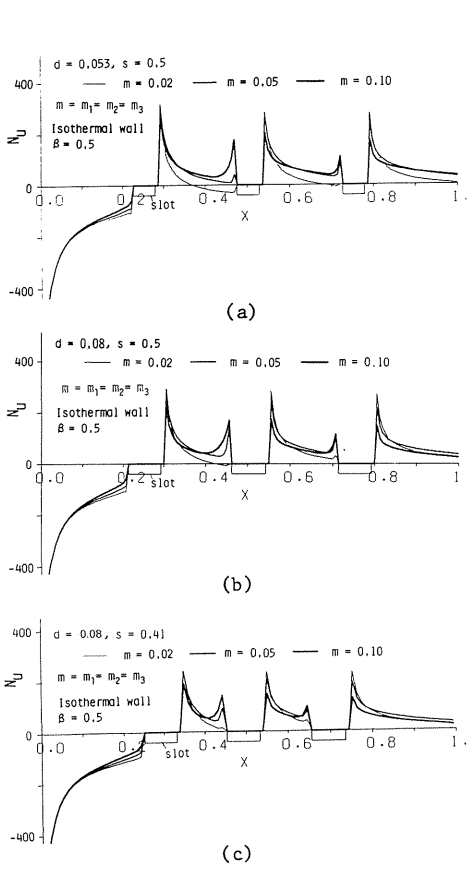

Fig. 14 Variations of *Nu* along isothermal wall with slots.

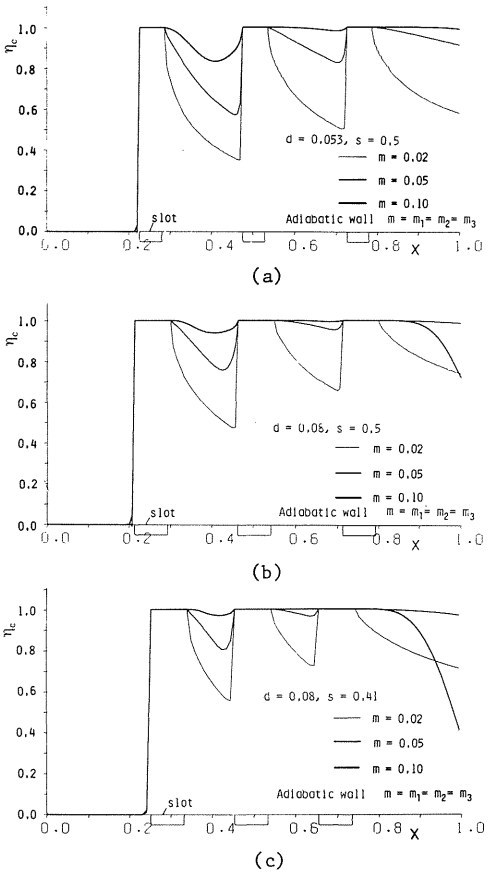

Fig. 15 Variations of η_c along adiabatic wall with slots.

Figs. 14 (a) to (c) show variations of *Nu* (eq. (13)) on the isothermal wall with *d*, *s* and *m*. Generally speaking, an increase in *m* increases *Nu*, but an increase in *Nu* saturates at a value of *m*. *Nu* is very large near the leading and trailing edges of all the slots except near the leading edge of the 1st slot, and is larger near the slot trailing-edges than near the slot leading-edges. The regions of the large *Nu* have the good correlation with those of the large ζ. However, *Nu* is smaller in the central part between the slots than near the leading and trailing edges of each slot. Figs. 14 (a) to (b) also indicate that an increase in *d* or a decrease in *s* increases *Nu*, and a negative *Nu* grows in the regions among the three slots at a small *d* (=0.053), but it only occurs in the region between the 1st and 2nd slots at *d*=0.08 (cf. Figs. 14 (b) and (c)).

Figs. 15 (a) to (c) show variations of η_c (eq. (14)) on the adiabatic wall with *d*, *s* and *m*. Figs. 15 (a) and (b) show that an increase in *d* increases η_c. Figs. 15 (b) and (c) show that a decrease in *s* also increases η_c. This is reasonable, because we know empirically that η_c becomes high at a large *d* and a small *s*. We see also that η_c is large near the slot trailing-edge, and is small near the slot leading-edge.

The present simulation is carried out at small velocity ratios m's ($\leq 0.1 \sim 0.2$). This comes from a difficulty of convergence in the iteration process for the calculation of ψ. The situation is directly attributable to a great cross-flow-wise change of the v component at the slot leading and trailing-edges from a small value within the cross flow to a large value in the blowing flow, because we use the boundary condition which gives a uniform blowing velocity at slot exit. Such a boundary condition also is not correct experimentally. However, this situation can be improved, when it is taken that the velocity of the blowing fluid is uniform far upstream of the slot exit. This treatment reduces the great cross-flow-wise change of the v component at the leading and trailing edges of the slot exit, because the boundary layer grows on the blowing-pipe wall and the blowing velocity vector changes its direction in the blowing-pipe upstream of the slot exit by the action of the cross flow. This will bring about an increase in m more than $0.1 \sim 0.2$. It is believed that this improved boundary condition is near an actual situation.

We try to obtain the increase in m by other finite-difference scheme without using the $\psi-\zeta$ system.

4. Conclusions

It is revealed that the present analysis gives qualitatively reasonable results, but the results must be verified experimentally. Results are summarized as follows.

1. When m is fixed, the recirculating region between the slots is smaller in the downstream part of the wall than in the upstream one. An increase in m expands the recirculating region. A decrease in s or d results in a reduction of the recirculating regions.
2. The acceleration of the plume fluid due to cross flow is greater at the leading edge of the plume than in the inside. This shows the progress of the mixing of the injectant and the cross flow.
3. There is a large decrease in c_f on the slotted wall, as m increases, and the boundary-layer velocity profiles have a tendency to separation in every place on the slotted wall. The magnitude of d has a predominant effect on c_f through the flow rate of the injectant.
4. Effects of the recirculating flow are clearer in isotherms near the isothermal wall than near the adiabatic wall. The adiabatic wall causes the injectant to accumulate near the wall.
5. The local heat transfer coefficient is very large near the leading and trailing edges of the slots. There is the minimum heat transfer coefficient between the slots.
6. An increase in d or a decrease in s increases Nu and η_c on the slotted wall.

References

1) Bahl, R., Boundary-layer blowing, AIAA J., 23-1, 157–158 (1985).
2) Roache, P.T., Computational fluid dynamics, Hermasa publishers, 48–53 (1972).
3) Takahashi, R. et al., Computational fluid dynamics (Exercises), Institute of structure planning, 36–52 and 148–149 (1982) (in Japanese).
4) Fujimoto, B. and Sato, S., Introduction to heat transfer, Kyoritsu-Shuppan, Tokyo, 127 (1956) (in Japanese).
5) Jones, W.P. and McGuirk, J.J., Computation of a round turbulent jet discharging into a confined cross-flow, Turbulent Shear Flow 2, Springer-Verlag, 233–245 (1980).

6) Bergeles, G., Gosman, A.D. and Launder, B.E., The prediction of three-dimensional discrete-hole cooling processes, Part 1: Laminar flow, Trans. ASME, J. of Heat Transfer, Ser. C, 98-3, 379–386 (1976).
7) Bergeles, G., Gosman, A.D. and Launder, B.E., The prediction of three-dimensional discrete-hole cooling processes, Part 2: Turbulent flow, Trans. ASME, J. of Heat Transfer, 103-1, 141–145 (1981).